TABLE V. Comparison of the experimental magnetic moment results with theory.

Nucleus	E (keV)	Theory: Kumar and Baranger $g/g(194)$	Theory: Kumar and Baranger g	Theory: Greiner $g/g(194)$	Theory: Greiner g	Experiment $g/g(194)$	Experiment g
Pt^{192}	316	0.969	0.284	1.013	0.311	0.88±0.05	0.28±0.03[a]
Pt^{194}	328.5	1.000	0.293	1.000	0.307	1.00	0.32±0.04[b]
Pt^{196}	355.7	1.027	0.301	0.99	0.303	0.84±0.05	0.27±0.04[b]
Pt^{198}	408			0.98	0.299	0.87±0.06	0.28±0.04[b]

[a] Using average $\omega\tau$ from Refs. 6–8; $H_{\text{int}}(\text{static}) = -(1.21\pm0.05)\times10^6$ G; $\tau = 51\pm4$ psec [A. Schwarzschild, Phys. Rev. **141**, 1206 (1966)].
[b] Present work.

moments obtained in that way show very slight changes going from Pt^{192} to Pt^{198}, and are given in column 4 of Table V. A different theoretical approach to the transition region is given by Greiner's rotational-vibrational model. In this model it is assumed that the difference in the pairing force of protons and neutrons causes different deformations for the protons and neutrons in the nucleus. The relative deformation is related to the strength of the pairing force by $\beta_0(p)/\beta_0(n) = (G_n/G_p)^{1/2}$. The g factors of rotational states are given by Greiner as

$$g = (Z/A)(1-2f),$$
$$f = [\beta_0 - \beta_0(p)]/\beta_0, \quad \beta_0 = [N\beta_0(n) + Z\beta_0(p)]/A.$$

Taking $G_n = 20A^{-1}$, $G_p = 30A^{-1}$, one gets g values, Table V, which show a slight decrease with neutron number. The accuracy of the present results is not sufficient to discriminate between the small differences in the isotopic trend as predicted by both theories. Much more accurate measurements of the lifetimes, the precession angles, and the internal fields are needed for such a discrimination.

ACKNOWLEDGMENTS

Two of us (R.K. and L.G.) wish to express our thanks to the University of Wisconsin Physics Department for its hospitality. One of us (B.H.) acknowledges a NATO travel grant. The help of R. Nord, G. Cohn, W. Roney, and P. Ryge in collecting the data is appreciated.

PHYSICAL REVIEW VOLUME 161, NUMBER 4 20 SEPTEMBER 1967

Elastic Scattering of ^{12}C, ^{14}N, and ^{16}O by ^{208}Pb and of ^{16}O by ^{209}Bi†*

S. D. BAKER‡ AND J. A. MCINTYRE§
Yale University, New Haven, Connecticut
(Received 15 May 1967)

Differential cross sections have been measured for elastic scattering of ^{12}C, ^{14}N, and ^{16}O by ^{208}Pb and of ^{16}O by ^{209}Bi. A phase-shift analysis of the data was made to evaluate the nuclear interaction radius R and the "surface thickness" for the interaction ΔR. The interaction-radius parameter r_0 was found to be 1.44±0.03 F for all four scattering experiments, where $R = r_0(A_1^{1/3} + A_2^{1/3})$, the A_i being the nuclear masses of the two nuclei involved in the scattering process. In contrast to the constant value found for r_0, the "surface thickness" was found to be 0.31±0.02 F for the ^{14}N scattering, 0.42±0.04 F for the ^{16}O scattering on both ^{208}Pb and ^{209}Bi, and 0.49±0.05 F for the ^{12}C scattering. It is not clear why these "surface thicknesses" differ as they do.

I. INTRODUCTION

SINCE the advent of accelerators capable of supplying enough energy to light nuclei (heavy ions) to overcome the Coulomb barrier of nuclei of atoms high in the periodic table, it has been hoped that elastic-scattering studies using these projectiles would be sensitive probes of nuclear properties, especially in the surface regions of the two colliding systems. One reason for this hope was that the value of the parameter

$$\eta = ZZ'e^2/\hbar v \qquad (1)$$

is large (10 to 30), indicating that classical or semiclassical theories would be applicable.[1] (Here, Ze and $Z'e$ are the electric charges of the target and projectile nuclei, $2\pi\hbar$ is Planck's constant, and v is the relative velocity between the projectile and target nuclei.)

† Supported by the U. S. Atomic Energy Commission.
* Material supplementary to this article has been deposited as Document No. 9534 with the ADI Auxiliary Publications Project, Photoduplication Service, Library of Congress, Washington, D. C. 20540. A copy may be secured by citing the document number and by remitting $1.25 for photoprints, or $1.25 for 35 mm microfilm. Advance payment is required. Make checks or money orders payable to: Chief, Photoduplication Service, Library of Congress.
‡ Present address: William Marsh Rice University, Houston, Texas.
§ Present address: Texas A&M University, College Station, Texas.

[1] See, e.g., E. J. Williams, Rev. Mod. Phys. **17**, 217 (1945).

Thus, one could perhaps extract information about the nuclear size and surfaces in a classical manner. In addition, the energies available (up to $\approx$10 MeV/amu), together with the complexity of the colliding systems, makes the number of accessible reaction channels very large, so that a strong absorption picture of the scattering process should be plausible.

Such a viewpoint is incorporated into the so-called sharp-cutoff model,[2] which represents the scattering process as the complete removal from the outgoing wave of partial waves with values of the angular-momentum quantum number lower than some cutoff value l' which corresponds to the classical trajectory for grazing collision. To each value of l there corresponds a classical orbit for which the distance of closest approach r_l is given by the semiclassical expression[2]

$$l(l+1)=(2\mu r_l^2/\hbar^2)(E_{\text{c.m.}}-(ZZ'e^2/r_l)). \quad (2)$$

(Here, μ is the reduced mass of the projectile and $E_{\text{c.m.}}$ is the energy of the reaction in the center-of-mass system.) An interaction radius $R=r_{l'}$ may thus be obtained.

This model has been very useful in fitting angular distributions of alpha-particle and heavy-ion scattering for the purpose of obtaining nuclear radii, since only one parameter (l') is needed. However, experiments with alpha particles[3] and heavy ions[4–6] at laboratory energies of $\approx$10 MeV/amu over a wide range of targets have indicated that the nuclear radius of interaction, obtained from sharp-cutoff-model fits, can be expressed as $R=r_0(A_1^{1/3}+A_2^{1/3})$, where r_0 varies very little from 1.45 F over all the experiments.[7] (Here, the A_i are the nuclear masses in amu of the target and projectile nuclei.) This constant value for r_0 indicates that experiments in which only the nuclear radius is obtained will give very little information on nuclear structure.

Modification of the sharp-cutoff model has been successful in describing the experimental angular distributions with much better accuracy.[8] The modification consists of replacing the sharp cutoff in l space with a smooth transition from complete absorption to no absorption. A smoothed real phase shift is also needed to describe adequately the elastic scattering.

From the range Δl of l values over which this smooth transition takes place one can determine an absorption surface thickness ΔR by (again) assuming classical orbits and differentiating Eq. (2),

$$\Delta l(2l'+1)=(2\mu/\hbar^2)(2E_{\text{c.m.}}R-ZZ'e^2)\Delta R. \quad (3)$$

The relation between this procedure for fitting data and others, such as the optical model, is discussed by several authors as is the physical meaning of the R and ΔR obtained from such phase-shift analysis.[2,9]

The work reported here is an attempt to elucidate the problem of whether information concerning the surface thickness can be obtained from heavy-ion scattering. Previous efforts along these lines[10,11] have been experimentally inconclusive primarily because in most cases inelastic scattering could not be unambiguously separated from elastic scattering. Other difficulties with previous data include inadequate angular resolution and the fact that some data cannot be fitted with sufficient precision to provide quantitative conclusions.

In an attempt to circumvent these difficulties we have taken data in which (1) elastic scattering is distinguished from inelastic scattering, (2) angular resolution is $\approx$0.6° full width at half-maximum, and (3) the parameters used to fit the data can be determined with an improvement in precision over that of previous work.

The reactions studied were the elastic scattering of ^{16}O, ^{14}N, and ^{12}C by ^{208}Pb, and ^{16}O by ^{209}Bi at $\approx$10.45-MeV/amu bombarding energy. It is found that there are quantitative differences in the surface interaction thickness in the scattering from lead, the ΔR for the carbon scattering being approximately half again as large as that for the nitrogen scattering.

II. EXPERIMENT

A. Deflection System

It was our experience that the energy of the Yale heavy-ion-accelerator beam varied over a range of several percent. In order to be sure that the energy in our experiment remained constant to within a fraction of 1%, regardless of the accelerator adjustment, a modification of the existing deflecting system[12] was

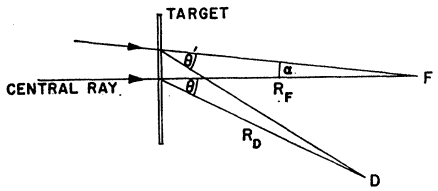

FIG. 1. Illustration showing quantities relevant to Eq. (4).

[2] J. S. Blair, Phys. Rev. **95**, 1218 (1954).
[3] A review of alpha-particle scattering experiments may be found in R. M. Eisberg and C. E. Porter, Rev. Mod. Phys. **33**, 190 (1961).
[4] A. Zucker, Ann. Rev. Nucl. Sci. **10** (1960).
[5] See D. D. Kerlee, H. L. Reynolds, and E. Goldberg, Phys. Rev. **127**, 1224 (1962), which contains reference to earlier work.
[6] E. Newman, P. G. Roll, and F. E. Steigert, Phys. Rev. **122**, 1842 (1962); A. M. Smith and F. E. Steigert, *ibid.* **125**, 988 (1962).
[7] At lower energies the radius parameter r_0, obtained from sharp-cutoff fits to the data, is larger. A. Zucker and M. L. Halbert, in *Proceedings of the Second Conference on Reactions between Complex Nuclei*, edited by A. Zucker *et al.* (John Wiley & Sons, Inc., New York, 1960), p. 144; D. A. Bromley, J. A. Kuehner, and E. Almqvist, *ibid.*, p. 151.
[8] J. A. McIntyre, K. H. Wang, and L. C. Becker, Phys. Rev. **117**, 1337 (1960).
[9] J. Alster and H. E. Conzett, Phys. Rev. **139**, B50 (1965), and references therein.
[10] J. Alster and H. E. Conzett, Phys. Rev. **136**, B1023 (1964).
[11] J. A. McIntyre, S. D. Baker, and K. H. Wang, Phys. Rev. **125**, 584 (1962).
[12] E. R. Beringer, Yale Heavy-Ion-Accelerator Design Note No. 21, 1960 (unpublished).

designed which consisted of two 45° deflecting magnets, beam defining slits, and no quadrupole focusing lenses. The calculated distribution in energies emerging from the system was roughly triangular with the full width at half-maximum being 0.25%.

B. Scattering Chambers

Two scattering chambers were used. The first[13] (used for the data taken with oxygen and nitrogen beams, and hereafter referred to as chamber I) incorporated a detector moving on a circle of 21.9-in. radius outside the chamber vacuum. Particles scattered by the target reached the detector by passing through a 0.001-in. Mylar window on the scattering chamber, a 1-in. air gap, and a 0.00025-in. aluminized Melinex window on the detector's separate vacuum system. A monitor detector which was not movable was used in the experiment, and this was also mounted outside the chamber. The second apparatus[14] (used for the data taken with the carbon beam and hereafter referred to as chamber II) superseded the first and allowed both detectors to be mounted inside the chamber vacuum. One detector was movable on a circle of radius 20.5 in. The monitor detector was fixed. In both systems the angular position of the movable counter was reproducible to $\pm 0.02°$ and the estimated limits of systematic error in the measurement of the angle between two settings of the goniometer were: chamber I, $+0.025\%$ and -0.08%; chamber II, $\pm 0.06\%$ of the angular measure from 0°. Aluminum and nickel foil stacks increasing in ≈ 0.5 mg/cm^2 (aluminum equivalent) steps could be placed in the beam ahead of the target for the purpose of measuring the energy at the target through the use of range-energy relations.[15] Antiscattering baffles were placed so that the target-out counting rate was negligible.

C. Beam Centering

The adjustment of the accelerator parameters affected the direction in which the beam entered the scattering chamber; this effect would have introduced systematic shifts in the scattering angle of as much as 0.2°. The demands on the precision of the scattering angle were therefore met in the following way: First, consider Fig. 1, which shows the central beam ray and another ray meeting it at a point F, a distance R_F beyond the target, at an angle α. If particles are scattered out of these rays by a target set perpendicular to the central ray into a detector at point D, at a distance R_D from the center of the target, the difference in the angles through which the beam particles are scattered is given by

$$\delta\theta=\theta-\theta'=(\theta+\alpha)-\tan^{-1}(R_D^{-1}R_F\tan\alpha\sec\theta+\tan\theta), \quad (4)$$

which is zero to first order in α and θ if $R_F=R_D$. This effect was employed in the experiment by placing a small magnet between the entrance slit and the target to steer the beam so that it would cross the center line at a point beyond the target. The position of the beam at this crossing point was determined by a split beam stopper. The difference of the output signals from the two sides of the beam stopper was displayed on an oscilloscope. The current through the steering magnet was adjusted so that the oscilloscope trace produced a curve that integrated to zero over a beam pulse. This integration, made visually, was estimated to be sufficiently accurate to insure that no less than 35% of the total beam was striking either plate of the beam stopper. This corresponds to an angular precision of about 0.05° in our apparatus.

By using the steering magnet to sweep the beam across the beam stopper, an estimate of the beam intensity along the beam stopper was made which, when folded into the contribution to angular resolution from the detector size, gave a direct measure of the angular resolution of the experiment. This measurement was in substantial agreement with the calculation of angular resolution described below. The estimate of angular precision mentioned in the paragraph above is also obtained from this measurement.

D. Angular Resolution

In determining the angular resolution of the experiment the effects of the following experimental factors were evaluated: (1) the divergence and size of the beam at the entrance slit of the scattering chamber (calculated from the properties of the deflection system mentioned above); (2) the size of the detector slit; (3) multiple scattering in the target and in the window of chamber I; and (4) spread in beam energy.[16] The angular resolutions (full width at half-maximum) obtained in this fashion were 0.5° for the oxygen and nitrogen scattering and 0.7° for the carbon scattering.

E. Targets

The targets were prepared by evaporating lead or bismuth metal onto less than 50-μg/cm^2 Formvar films. The lead, supplied by Oak Ridge National Laboratory, was 99.75% ^{208}Pb. The thicknesses, obtained by weighing, were: ^{209}Bi target, 0.55 mg/cm^2; ^{208}Pb target, 0.47 mg/cm^2. These correspond to energy losses of 0.34 and 0.29 MeV, respectively, in the case of 170-MeV ^{16}O ions.

[13] This chamber is similar to the chamber described in Ref. 11 except that an extension was built so that, to reduce the effect of multiple scattering, the window would be further from the target.

[14] K. H. Wang and J. A. McIntyre, Phys. Rev. **139**, 1231 (1965).

[15] L. C. Northcliffe, Ann. Rev. Nucl. Sci. **13**, 67 (1963); Natl. Acad. Sci.—Natl. Res. Council, Publ. **1133** (1964); (private communication).

[16] J. A. McIntyre, S. D. Baker, and T. L. Watts, Phys. Rev. **116**, 1212 (1959).

F. Electronics and Beam Monitoring

Two detectors were used in taking data: a monitor counter, set at $\approx 20°$, and a movable counter which could be positioned on both sides of zero at small angles and out to larger angles on one side of zero. With chamber I a CsI scintillation crystal viewed by a photomultiplier tube was used for the monitor counter, and a silicon junction detector was used for the movable counter. With chamber II a silicon junction detector and a silicon surface-barrier detector were used for the monitor and movable counters, respectively. After amplification, the monitor counter pulses passed into a lower-level discriminator. The pulses from the discriminator and the pulses from the movable counter's amplifier were fed into an RIDL 400-channel analyzer. Gains were adjusted so that the discriminator pulses from the monitor counter fell in higher channels than pulses from the movable counter.

G. Beam-Energy Determination

The energies of the ^{16}O and ^{14}N beams were obtained by measuring the thickness of aluminum required to reduce the transmitted beam current to zero. The data of Northcliffe[15] relate this measurement to the energy. Errors in this method arise from the errors quoted by Northcliffe and the uncertainty in extrapolating to zero current. The energy of the ^{12}C beam was obtained by calibrating a surface-barrier detector with alpha particles from a Th C-C' source, and then measuring the energy of the heavy ions after they had been scattered by a thin lead target through 16° and reduced in energy to below 20 MeV by means of aluminum absorbers. Again using Northcliffe's data for the aluminum absorber, the full energy of the beam was determined. The chief source of the assigned error in this measurement was the lack of knowledge of the thickness of the dead layer of the detector. The beam energies determined as described above were: ^{16}O, 170.1±1.7 MeV; ^{14}N, 146.7±0.5 MeV; ^{12}C, 125.3±0.5 MeV. It should be remembered that the actual spread in the beam energy (see Sec. IIA above) was considerably smaller than the precision with which the mean energy was determined.

H. Zero-Scattering-Angle Determination

The angle corresponding to zero-angle scattering was determined by measuring the elastic scattering at several small angles ($\approx 5°$ to 15°) on both sides of zero. These data yielded symmetrical curves, from which the measured zero angle was determined to be almost certainly within ±0.1° of the true zero scattering angle. To be sure that this estimate was not over-optimistic, one case (the ^{12}C run) was studied in detail. The likelihood function[17] was computed for several choices of the zero angle and it was found that one could assign the zero angle to ±0.1° with 99.7% probability.

I. Measuring the Angular Distribution

One angular setting was repeated often to insure against undetected drifts in the electronics and other sources of nonreproducibility. The angular range above ±20° was swept through at least twice so that systematic shifts with time might also be detected in this way. When scattering chamber I was used, two fixed apertures, behind which the monitor counter could be placed, were available so that the counting rates from the monitor and movable counters remained roughly equal as the movable counter was changed in angle.

J. Determination of Elastic Scattering

Figure 2 shows a representative pulse-height spectrum taken at large angles in the ^{16}O on ^{208}Pb reaction. The peak due to monitor counts is off the figure at higher channels. The channel corresponding to $Q=-2.6$ MeV (excitation of the first excited state in lead) is indicated. Similar spectra were obtained for the ^{14}N and ^{12}C on ^{208}Pb and ^{16}O on ^{209}Bi reactions.

Superimposed is a solid curve indicating the pulse-height spectrum taken at smaller angles, which has been shifted to lower channels to line up with the large-angle data. This curve may be considered the instrumental line shape of the apparatus since it gives the pulse-

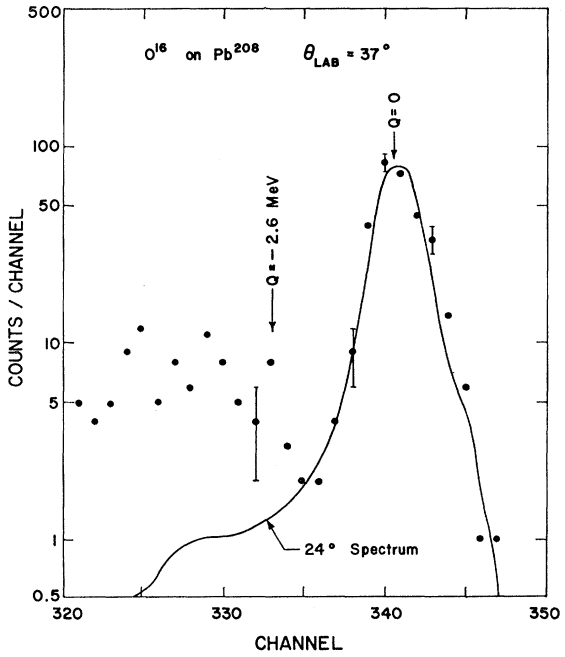

FIG. 2. Representative pulse-height spectrum taken with the movable detector at a laboratory angle of 37° in the ^{16}O in ^{208}Pb reaction. Superimposed is the shape of the spectrum at 24°. The position of a peak which would correspond to inelastic scattering with $Q=2.6$ MeV is indicated.

[17] See, e.g., H. Cramér, *Mathematical Methods of Statistics* (Princeton University Press, Princeton, New Jersey, 1951).

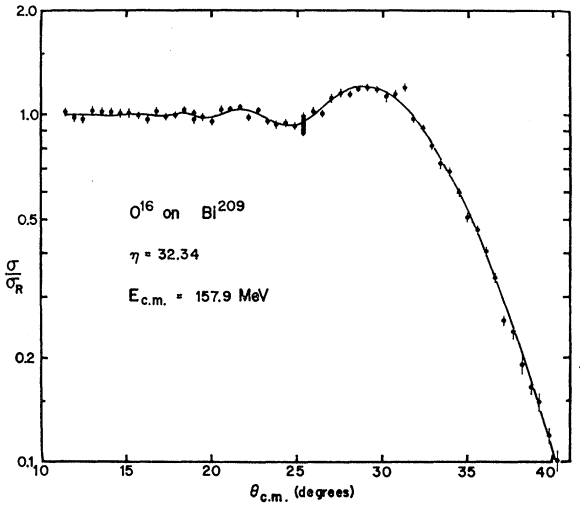

FIG. 3. Ratio of the differential elastic-scattering cross section to Rutherford scattering: ^{16}O on ^{209}Bi, $\eta=32.34$, $E_{c.m.}=157.9$ MeV. The smooth curve is calculated from parameters listed in Table I.

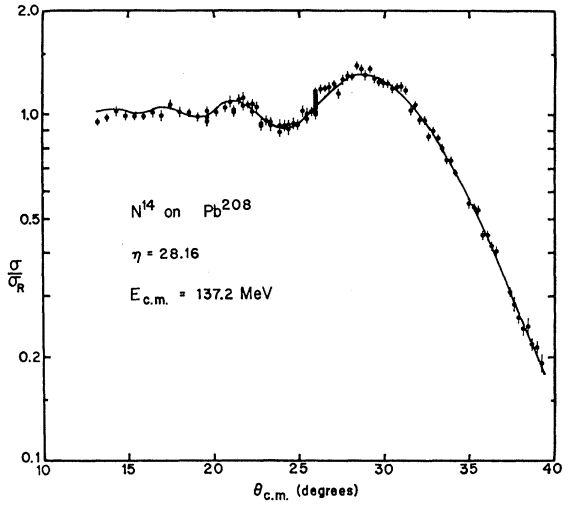

FIG. 5. Ratio of the differential elastic-scattering cross section to Rutherford scattering: ^{14}N on ^{208}Pb, $\eta=28.16$, $E_{c.m.}=137.2$ MeV. The smooth curve is calculated from parameters listed in Table I.

height spectrum at small angles where elastic scattering is expected to dominate completely. The shape of the high-energy side of the peak is the same for all angles indicating that the observed shape is due to elastic scattering and is instrumental in origin.

Because of the length of the low-energy "tail" on the peaks, it is difficult to determine exactly how many counts are due to elastic scattering. However, it is possible to determine the fraction of the sum of all the channels down to, say, 10 channels below the elastic peak which can be attributed to elastic scattering, and since we are measuring relative cross section only, this is what was done.

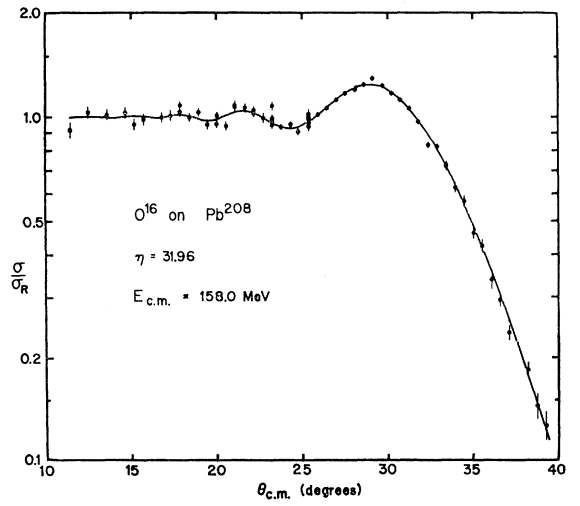

FIG. 4. Ratio of the differential elastic-scattering cross section to Rutherford scattering: ^{16}O on ^{208}Pb, $\eta=31.96$, $E_{c.m.}=158.0$ MeV. The smooth curve is calculated from parameters listed in Table I.

In the case of ^{16}O on ^{209}Bi the first excited state was too close to the ground state to make possible an unambiguous distinction between elastic and inelastic scattering. However, an upper limit of 10 to 20% of the elastic scattering could be assigned to scattering leading to excitation of the 0.79 and 1.58 MeV levels, and in all cases the data were entirely consistent with no inelastic contribution. It may be argued, moreover, that because of the single-particle nature of these states[18] their excitation by heavy-ion bombardment would be small.

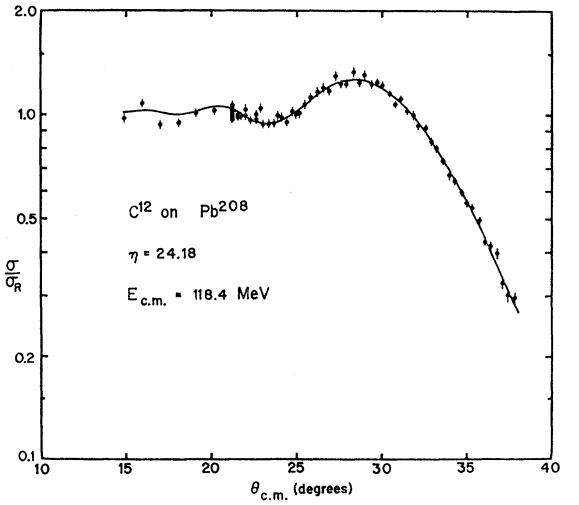

FIG. 6. Ratio of the differential elastic-scattering cross section to Rutherford scattering: ^{12}C on ^{208}Pb, $\eta=24.18$, $E_{c.m.}=118.4$ MeV. The smooth curve is calculated from parameters listed in Table I.

[18] J. S. Blair, D. Sharp, and L. Wilets, Phys. Rev. 125, 1625 (1962).

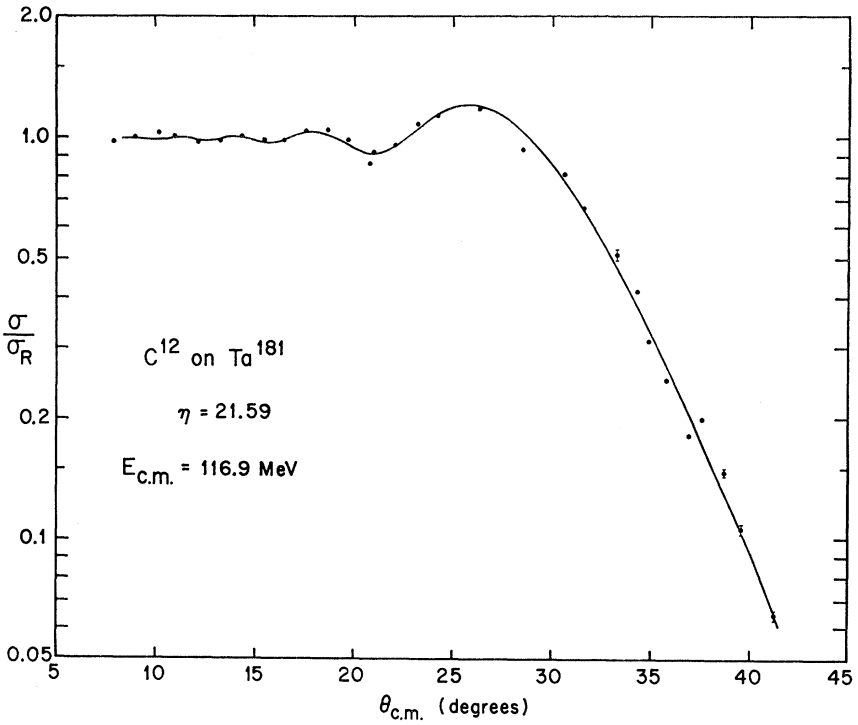

FIG. 7. The data of Alster and Conzett (Ref. 20) for the ratio of the differential elastic-scattering cross section to Rutherford scattering: ^{12}C on ^{181}Ta, $\eta=21.59$, $E_{c.m.}=116.9$ MeV. The smooth curve is calculated from parameters listed in Table I.

In the cases of scattering from ^{208}Pb it was possible to set an upper limit of 1 to 2% of elastic scattering for the cross section of processes with $-3\leq Q\leq -2$ MeV. It therefore seems reasonable to estimate that the accuracy of determining the relative number of elastic events from the pulse-height spectra is better than $\pm 2\%$ over the entire range of angles.

K. Reduction of the Data

The number of elastic events was divided by the number of monitor counts to give the relative laboratory differential cross section. Since two different monitor apertures were used in the course of taking an angular distribution[19] it was necessary to determine the multiplication factor required to bring the two sets of (overlapping) data into register. Because it was difficult to measure the apertures to better than 2% and to know exactly what geometrical correction to make to obtain an effective aperture size, the multiplication factor of maximum likelihood[17] was determined from the data, using the Yale IBM-709 computer. The uncertainty (a standard deviation of approximately 1%) in the multiplication factor was folded into the statistical errors in the small-angle data. The data were then transformed to the center-of-mass system.

The values of the ratio of the center-of-mass cross section to the Rutherford scattering cross section are plotted in Figs. 3 through 6. The errors shown are statistical errors (standard deviation) only. The points which were used as check points have been left un averaged as an indication of the reproducibility of the experiment. The data have been normalized to unity at small angles by eye. The solid curves are the results of calculations described in the following section.

[19] Except in the case of the ^{12}C on ^{208}Pb run.

III. ANALYSIS OF THE DATA

The angular distributions obtained were parametrized by means of the modification of the sharp cutoff calculation[8] mentioned in the Introduction and described below. For purposes of comparison, a similar analysis of the ^{12}C on ^{181}Ta scattering data of Alster and Conzett[20] (Fig. 7) has also been carried through.

The ratio of the center-of-mass differential cross section σ to the Rutherford scattering cross section σ_R may be written, for spin-zero particles,

$$\sigma/\sigma_R=|-i\exp\{-i\eta\ln[\sin^2(\theta/2)]\}$$
$$-\eta^{-1}\sin^2(\theta/2)\sum_{l=0}^{\infty}[1-A_l\exp(2i\delta_l)]$$
$$\times(2l+1)P_l(\cos\theta)\exp[2i(\sigma_l-\sigma_0)]|^2.$$

Here θ is the scattering angle, η is given by Eq. (1), $P_l(\cos\theta)$ is the lth Legendre polynomial, and σ_l is the Coulomb phase shift, where

$$\sigma_l-\sigma_{l-1}=\tan^{-1}(\eta/l).$$

[20] University of California Radiation Laboratory Report No. 9650 (unpublished). It should be noted that the tabulated values in this reference disagree in minor details with those reported by J. Alster and H. E. Conzett, Phys. Rev. **136**, B1023 (1964); however, results of the data analysis reported in this paper are identical to those in the UCRL report.

TABLE I. Parameters of the reactions studied.

	$^{16}O+^{209}Bi$	$^{16}O+^{208}Pb$	$^{14}N+^{208}Pb$	$^{12}C+^{208}Pb$	$^{12}C+^{181}Ta$[a]
$l_A=l_\delta$	91.65±0.43	90.95±0.38	79.00±0.19	66.32±0.66	65.30±0.45
$\Delta l_A=\Delta l_\delta$	4.85±0.45	4.75±0.38	3.05±0.23	4.20±0.45	3.05±0.47
δ_0	0.56±0.05	0.66±0.05	0.59±0.03	0.68±0.06	0.37±0.08
Degrees of freedom	52	47	84	56	26
χ^2_{min}	58	53	93	63	735
E_{lab} (MeV)	170.1	170.1	146.7	125.3	124.5
R (F)	12.23±0.04	12.13±0.04	12.08±0.02	11.85±0.08	11.43±0.06
r_0 (F)	1.447±0.005	1.436±0.004	1.450±0.003	1.440±0.010	1.439±0.008
ΔR (F)	0.43±0.04	0.42±0.04	0.31±0.02	0.49±0.05	0.36±0.06

[a]See Ref. 21.

Nuclear effects in the scattering are introduced through A_l and δ_l, whose functional form is given by

$$A_l=\{1+\exp[(l_A-l)/\Delta l_A]\}^{-1},$$
$$\delta=\delta_0\{1+\exp[(l-l_\delta)/\Delta l_\delta]\}^{-1}.$$

There are thus five parameters which are at our disposal with which we may try to fit the angular-distribution data: l_A, l_δ, Δl_A, Δl_δ, and δ_0. In the work described below the freedom of two of these parameters was eliminated by setting $l_A=l_\delta$ and $\Delta l_A=\Delta l_\delta$. In those cases tried, allowing l_δ and/or Δl_δ to vary independently did not give statistically significant improvements in the fits. However, searches for the best sets of more than three free parameters were not completed, so that it cannot be asserted that more than three free parameters would not give better fits to the data.

The quality of fit was indicated by the smallness of χ^2, where

$$\chi^2=\sum_i\{[\sigma_{calc}(\theta_i)-\sigma_{exp}(\theta_i)]/\Delta\sigma(\theta_i)\}^2.$$

Here $\sigma_{calc}(\theta_i)$, $\sigma_{expt}(\theta_i)$, and $\Delta\sigma(\theta_i)$ are the cross sections calculated with a particular choice of the three parameters, the observed cross sections, and the experimental (counting statistics) error, respectively, for each angle θ_i measured in the angular distribution. To eliminate any dependence on the arbitrary normalization of the data to Rutherford scattering, the normalization was automatically adjusted to give the minimum value of χ^2 for each set of parameters in the calculation. The data taken at angles used for checking repeatability were excluded in the parameter searches so as not to give those angles excessive weight.

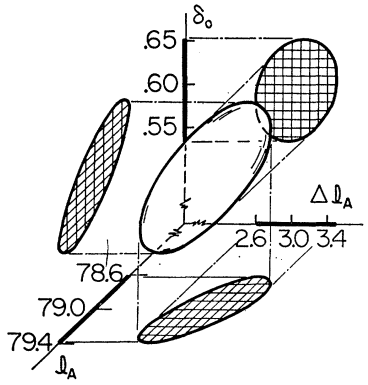

FIG. 8. A three-dimensional plot of the χ_2^2 contour in parameter space. (χ_2^2 represents the values of the parameters corresponding to two standard deviations away from their optimum values, the values giving a minimum χ^2.) The projections on the parameter axes are twice the standard deviations quoted for the parameter values in Table I. Also shown by the crosshatched areas are the projections of the three-dimensional contour onto the three coordinate planes. The contour shown is for ^{14}N on ^{208}Pb.

For each reaction, a set of three parameters, $l_A=l_\delta$, $\Delta l_A=\Delta l_\delta$, and δ_0 was determined which gave a minimum value of χ^2. These minimum values χ^2_{min}, rounded off to integers, are shown in the fifth line of Table I. The number of degrees of freedom N shown in the fourth line is the number of experimental points fitted minus four (three parameters in the calculation plus one normalization factor). It is not surprising that in all cases the value of χ^2_{min} is larger than N since in computing χ^2 we have ignored errors in the data from causes other than statistics. However, the difference between N and χ^2_{min} is small, which shows that the systematic error is small.[21] The first three lines in Table I show the values of the parameters whose uncertainties were obtained in the following way: Values of χ^2 were calculated on points of a three-dimensional grid in parameter space. Then a surface of constant χ^2 was traced out and its projection on the coordinate axes noted. Such a procedure is shown for the case of ^{14}N on ^{208}Pb in Fig. 8. The choice of χ^2 to be used for the surface is somewhat arbitrary since approximately similar ellipsoids are obtained so long as the value of χ^2 is kept close to χ^2_{min}. The following procedure was followed in determining the value of χ^2 to be used for the surface. The relative likelihood[17] L of various fits may be estimated to be

$$L\propto\exp(-\chi^2_{eff}/2),$$

where χ^2_{eff} is an effective χ^2 which allows, at least in part, for the fact that N is smaller than χ^2_{min}: $\chi^2_{eff}=(N/\chi^2_{min})\chi^2$. The uncertainties in the mean values of

[21] The large value of χ^2_{min} obtained from Alster and Conzett's data for ^{12}C on Ta indicates that their data fluctuate for reasons other than statistics. Nonreproducibility in the scattering angle by as little as 0.1° could account for such fluctuations.

the three parameters $l_A=l_\delta$, $\Delta l_A=\Delta l_\delta$, and δ_0 are defined as being the values which reduce the magnitude of the likelihood function from its value for best fit to a value corresponding to one standard deviation away from the best fit. Thus,

$$\text{likelihood (best fit)}=\exp\left\{\frac{-\chi^2_{\text{eff(min)}}}{2}\right\}$$
$$=\exp(-N/2),$$

likelihood (one standard deviation away)

$$=\exp(-N/2)\exp(-\tfrac{1}{2})$$
$$=\exp(-\chi^2_{\text{eff}(1)}),$$

so that

$$\chi^2_{\text{eff}(1)}=(N/\chi^2_{\min})\chi_1^2=N+1,$$

and

$$\chi_1^2=\chi^2_{\min}+\chi^2_{\min}/N,$$

where χ_1 is the value of χ for a shift of one standard deviation in L. An ellipsoid in l, Δl, δ_0 space is thus determined for fixed χ_1^2. Such an ellipsoid is plotted in Fig. 8 except that the ellipse $\chi_2^2=$ constant for two standard deviations is shown instead for clarity. The value of χ_2^2 is

$$\chi_2^2=\chi^2_{\min}+4\chi^2_{\min}/N.$$

The uncertainties for l, Δl, and δ_0 listed in Table I, however, are those for one standard deviation and are defined as the value of the projections of the χ_1^2 ellipsoid on the l, Δl, and δ_0 axes, respectively.

Using Eq. (2), we can also calculate the value of R corresponding to l_A. These values of R, along with the corresponding values of $r_0=R/(A_1^{1/3}+A_2^{1/3})$, are listed in the next two lines of the table. The precision limits listed refer to the precision with which the parameters in the calculation were determined and does not include the precision of the beam-energy determination which enters directly into the computation of R and r_0 and so introduces an additional error of about 1% (see Sec. IIG). The angular error introduces only a few tenths of a percent error in the determination of R. Finally, using Eq. (3), values of ΔR corresponding to Δl_A are listed in the last line of Table I.

IV. DISCUSSION OF RESULTS

Reference to Table I shows that the value of r_0, the interaction-radius parameter, is remarkably constant for all the interactions studied. In fact, all the values of r_0 found are consistent with an average value of $r_0=1.44\pm0.03$ F. There appears, therefore, to be little information to be obtained about nuclear structure through a measurement of the interaction radius.

On the other hand, the "surface thickness" for the interaction, ΔR, does vary over a range of 40% (0.18 F) for the interactions studied. The most surprising feature of this variation is that the closed-shell projectiles, ^{12}C and ^{16}O, appear to have the thicker surface region. The same effect appears when ^{181}Ta and ^{208}Pb are compared with ^{12}C as the common projectile; the deformed ^{181}Ta nucleus appears to have a thinner surface region than the ^{208}Pb. This latter result is somewhat inconsistent with the results of McIntyre, Baker, and Wang,[11] who found that the surface thickness for the deformed ^{159}Tb nucleus in the ^{19}F+^{159}Tb interaction was larger than that for the ^{16}O+^{208}Pb interaction. However, because of the possible contribution of inelastic scattering in the ^{181}Ta and ^{159}Tb experiments, firm conclusions cannot be drawn from these scattering data. The differences between the ΔR values for ^{14}N, ^{12}C, and ^{16}O, on the other hand, are not subject to these limitations. It is interesting to note, too, that the surface thickness found for the ^{16}O as the projectile is the same for both the ^{208}Pb and the ^{209}Bi targets.

While the percentage difference in the surface thickness between ^{14}N and ^{12}C is large (over 40%), the magnitude of the difference is small (0.18 F). In terms of the nuclear interaction radius, $R\sim12$ F, the surface thickness in percent is $\Delta R/R\sim0.4/12\sim3\%$ and the variation in the thickness between ^{14}N and ^{12}C is only 1.5%. It is difficult to determine unambiguously the reason for an effect of this magnitude. A possible reason is that ^{12}C, as well as ^{16}O, is more "collective" and, hence, deformable than ^{14}N. However, ^{14}N has a spin of one while the other nuclei have no spin and this fact may contribute to the result found. One can only say with certainty that the difference in surface thickness is established experimentally.

V. CONCLUSIONS

The elastic scattering of ^{12}C, ^{14}N, and ^{16}O by ^{208}Pb has been studied as well as the elastic scattering of ^{16}O by ^{209}Bi. Nuclear interaction radii have been determined by a phase-shift analysis of the scattering process and a value of $r_0=1.44\pm0.03$ F has been found to be consistent with the scattering results for the four different experiments. In contrast to the remarkably constant value found for the radius parameter r_0, the "surface thickness" ΔR was found to be 0.31 ± 0.02 F for the ^{14}N scattering as compared to 0.49 ± 0.05 F for the ^{12}C scattering and 0.42 ± 0.04 F for the ^{16}O scattering. Because of the many structural differences between the nuclei involved in these interactions, it is difficult to assign, unambiguously, a reason for the small differences found in the surface-thickness parameter.

ACKNOWLEDGMENTS

We particularly wish to thank Dr. K. H. Wang for his assistance in taking the experimental data. Also, we appreciate the support of Professor E. R. Beringer in his position as Director of the heavy-ion accelerator facility.